USASP
US ASSOCIATION FOR THE STUDY OF PAIN

PUBLISHED BY
ELSEVIER

The Journal of Pain, Vol xxx, No. xxx (xxxx), xxxx: pp xxx–xxx
Available online at www.jpain.org and www.sciencedirect.com

Endothelial Glycocalyx in the Peripheral Capillaries is Injured Under Oxaliplatin-Induced Neuropathy

Takahiro Kuroda,[*,1] Akio Suzuki,[†,‡,1] Hideshi Okada,[§,¶,1] Masayoshi Shimizu,[*] Daichi Watanabe,[†] Keiko Suzuki,[†,‖] Kosuke Mori,[*,§] Kazufumi Ohmura,[*,**] Ayumi Niwa,[*] Yuko Imaizumi,[*] Mikiko Matsuo,[*] Koki Ichihashi,[*] Takafumi Okubo,[*] Toshiaki Taniguchi,[*] Tomohiro Kanayma,[*] Ryo Kobayashi,[†,‡] Shigeyuki Sugie,[††] Akira Hara,[*] and Hiroyuki Tomita[*,¶]

[*]*Department of Tumor Pathology, Gifu University Graduate School of Medicine, Gifu, Japan,* [†]*Department of Pharmacy, Gifu University Hospital, Gifu, Japan,* [‡]*Laboratory of Advanced Medical Pharmacy, Gifu Pharmaceutical University, Gifu, Japan,* [§]*Department of Emergency and Disaster Medicine, Gifu University Graduate School of Medicine, Gifu, Japan,* [¶]*Center for One Medicine Innovative Translational Research, Gifu University Institute for Advanced Study, Gifu, Japan,* [‖]*Department of Infection Control, Gifu University Graduate School of Medicine, Gifu, Japan,* [**]*Department of Neurosurgery, Gifu University Graduate School of Medicine, Gifu, Japan,* [††]*Department of Pathology, Asahi University Hospital, Gifu, Japan*

Abstract: **Oxaliplatin, a platinum-based anticancer drug, is associated with peripheral neuropathy (oxaliplatin-induced peripheral neuropathy, OIPN), which can lead to worsening of quality of life and treatment interruption. The endothelial glycocalyx, a fragile carbohydrate-rich layer covering the luminal surface of endothelial cells, acts as an endothelial gatekeeper and has been suggested to protect nerves, astrocytes, and other cells from toxins and substances released from the capillary vessels. Mechanisms underlying OIPN and the role of the glycocalyx remain unclear. This study aimed to define changes in the three-dimensional ultrastructure of capillary endothelial glycocalyx near nerve fibers in the hind paws of mice with OIPN. The mouse model of OPIN revealed disruption of the endothelial glycocalyx in the peripheral nerve compartment, accompanied by vascular permeability, edema, and damage to the peripheral nerves. To investigate the potential treatment interventions, nafamostat mesilate, a glycocalyx protective agent was used in tumor-bearing male mice. Nafamostat mesilate suppressed mechanical allodynia associated with neuropathy. It also prevented intra-epidermal nerve fiber loss and improved vascular permeability in the peripheral paws. The disruption of endothelial glycocalyx in the capillaries that lie within peripheral nerve bundles is a novel finding in OPIN. Furthermore, these findings point toward the potential of a new treatment strategy targeting endothelial glycocalyx to prevent vascular injury as an effective treatment of neuropathy as well as of many other diseases.**

Perspective: ***OIPN damages the endothelial glycocalyx in the peripheral capillaries, increasing vascular permeability. In order to prevent OIPN, this work offers a novel therapy approach that targets endothelial glycocalyx.***

Key words: *Endothelial glycocalyx, Neuropathy, Oxaliplatin, Peripheral capillary, Nafamostat mesilate*

Received August 28, 2023; Received in revised form December 2, 2023; Accepted January 3, 2024

[1]These authors contributed equally to this study.

Supplementary data accompanying this article are available online at www.jpain.org and www.sciencedirect.com.

Address reprint requests to Hiroyuki Tomita, Department of Tumor Pathology, Gifu University Graduate School of Medicine, 1–1 Yanagido, Gifu 501-1194, Japan. E-mail: tomita.hiroyuki.y6@f.gifu-u.ac.jp

1526-5900/$36.00

https://doi.org/10.1016/j.jpain.2024.01.005

Oxaliplatin, a third-generation platinum analog, is used to treat gastrointestinal cancers and colorectal cancer.[1] Oxaliplatin-induced peripheral neuropathy (OIPN) is a cumulative adverse event of oxaliplatin, characterized by dose-dependent severity and prolonged symptom duration.[2-5] OIPN can lead to impaired quality-of-life and changes or interruption of anticancer treatment. Convincing evidence supporting interventions that can prevent OIPN, are lacking, despite several clinical trials.[6]

Peripheral nerves encounter capillaries enveloped by the nerve fascicle and form the blood-nerve barrier.[7,8] This barrier is exposed to cells and molecules circulating in the blood, protecting endoneurial constituents (myelinated axons, resident macrophages, and fibroblasts) from toxic factors. In the blood-nerve barrier, capillaries or endoneurial blood vessels, are < 10 μm and are surrounded by endothelial cells, pericytes, and the basement membrane to provide oxygen, nutrition, cytokines, drugs, and other compounds to adjacent nerves.[7] Recently, the structural and functional importance of the blood-nerve barrier has been proposed, particularly in diabetic neuropathy and other peripheral nerve injuries.[9,8,10] Disruption of the barrier leading to increased vascular permeability and subsequent local inflammation may be associated with diabetic-neuropathy onset and progression.[8] Furthermore, in the peripheral-nerve compartment, only microvascular-capillary endothelial cells comprising the blood-nerve barrier are in direct contact with the systemic-circulation blood flow. Therefore, any barrier disruption due to oxaliplatin-induced vascular endothelial damage is hypothesized to be causative of OIPN, and prevention of blood-nerve barrier breakdown may be an ideal strategy to prevent OIPN.

The endothelial-cell luminal surface is covered in a glycocalyx composed of membrane-bound proteoglycans, glycoproteins, glycosaminoglycans, and adherent plasma proteins.[11] The endothelial glycocalx performs several functions necessary for vascular homeostasis, including vascular-permeability and microvascular-tone regulation, microvascular-thrombosis inhibition, and leukocyte adhesion and migration regulation in the endothelium.[12] The endothelial glycocalyx protects nerves, astrocytes, and other cells, from toxins and substances released from capillary vessels.[13-15] However, the mechanism by which oxaliplatin enters the vascular endothelium and the involvement of endothelial glycocalyx in this process are still not understood.

Three-dimensional-scanning electron microscopy images clearly visualize the glycocalyx and can define the vessel wall ultrastructures and surrounding environment abnormalities in normal organs[16,17] and cancer.[18]

This study defined changes in the three-dimensional ultrastructure of capillary endothelial glycocalyx near nerve fibers in hind paws of mice with OIPN. The effects of endothelial glycocalyx injury prevention in the OIPN were evaluated.

Methods

Mice

All animal experiments were performed in accordance with the guidelines of the Gifu University International Animal Care and Use Committee (no. 2020-104). For the in vivo study, male C57BL/6NCr Slc mice were obtained at 7 weeks of age from Japan CLEA, Inc (Hamamatsu, Japan) and were allowed to acclimatize for 1 week before the start of the experiment. The animals were kept in a normal light/dark cycles at 22 ± 1 °C and were fed a normal diet (CE-2, Japan CLEA, Inc) and autoclaved tap water. All behavioral experiments were conducted in the same room and in a randomized order before and after drug treatment. Body weight (g) was recorded every 7 or every 14 days, including the day of treatment and immediately before being euthanized. Mice were examined daily for abnormal clinical signs, such as piloerection, hindlimb weakness, gait disturbance, or gastrointestinal disorders, such as diarrhea.

Tumor-Bearing Mouse Model with Drug Treatments

To test the correlation between nafamostat mesilate and oxaliplatin treatment in a tumor-bearing mouse model, 8-week-old male C57BL/6NCr Slc mice (n = 10 per group) were used. Each mouse was subcutaneously inoculated with MC38 mouse colon cancer cells (1×10^6 cells/mouse) in the right dorsal flank. Tumors were measured with calipers every 1 or 2 weeks, and volumes (mm^3) were calculated using the following formula: $\pi/6 \times$ length $\times$ width $\times$ thickness. When subcutaneous tumors reached approximately 700 mm^3, the mice were randomly assigned to 4 groups: control-vehicle (G1), oxaliplatin-vehicle (G2), control-nafamostat mesilate (G3), and oxaliplatin-nafamostat mesilate (G4). A solution of 5% dextrose was the vehicle used to prepare oxaliplatin and nafamostat mesilate, which are water-soluble agents.

Mice in the control (G1) group received 5% dextrose during the experiment. The oxaliplatin (G2) group received oxaliplatin (5 mg/kg/mouse) dissolved in 5% dextrose twice per week for 5 weeks. The nafamostat mesilate (G3) group was administered nafamostat mesilate (30 mg/kg/day) dissolved in 5% dextrose daily. The oxaliplatin and nafamostat mesilate (G4) groups were administered oxaliplatin (5 mg/kg/mouse), and nafamostat mesilate (30 mg/kg/mouse/day) as indicated. The process was repeated weekly until the endpoint.

Assessment of Hypersensitivity (Mechanical Allodynia, von Frey Test)

Mechanical hypersensitivity thresholds were determined using the Dynamic Plantar Aesthesiometer (37,450, Ugo Basile, Italy) equipped with a von Frey-type diameter filament. In brief, each animal was placed in a Plexiglas chamber on an elevated mesh and acclimatized for at least 30 minutes. Mechanical force was applied in increasing

amounts to the ventral surface of the center of hind paw until the subject demonstrated a paw withdrawal response,[19] whereby the force was expressed in grams in each mouse at the indicated times.

Assessment of Hypersensitivity (Cold Allodynia, Acetone Test)

Cold allodynia was assessed using the acetone test, as previously described in ref.[20,21] Mice were put on a 25 × 25 cm plexiglass plate. A drop of acetone (50 μL) was administered to the mid-plantar region of the hind paw, and the number of nociceptive behaviors (shaking, lifting, licking, guarding, and biting) displayed by the hind paw were recorded for 1 minute.

Tissue Preparation

After anesthesia, the thorax of each mouse was exposed and the inferior vena cava was incised. Perfusion washing was performed using a drip infusion system with equal volumes of cold .1M PBS and 4% paraformaldehyde solution. The tissues were dissected, divided into pieces, and paraffin-embedded and frozen sections were prepared. The frozen and paraffin embedded blocks were cut into 5- and 3-μm thick sections, respectively, and subjected to hematoxylin and eosin staining as routine procedures.

Histological and Immunohistochemical Assays

Frozen sections were used for DyLight488-Tomato lectin and FITC-dextran staining. Fifteen minutes after injecting DyLight488-Tomato lectin (50 μg/100 μL dH_2O, VECTOR) or FITC-dextran (40,000 kDa, 200 μg/100 μL dH_2O, Sigma) through the jugular vein, tissues including mouse hind paws and tumors were removed and fixed in 4% paraformaldehyde overnight at 4 °C, incubated in 30% sucrose for cryoprotection (4 °C for 2–3 days), embedded in the optimal cutting temperature compound, and frozen with liquid nitrogen. Specimens were sectioned coronally at 5 μm using a cryostat (Leica), and each section was stored at –80 °C. For immunofluorescent staining, sections were incubated with rat anti-CD31 antibody (dilution 1:50, Dianova, Hamburg, Germany) or mouse anti-phosphorylated neurofilament heavy subunit (pNF-H) (dilution 1:100, Chemicon International, CA) overnight at 4 °C, followed by incubation with conjugated anti-rat Alexa594-conjugated secondary antibody (dilution 1:250, Abcam, Cambridge, UK, ab150084) for 60 minutes at 37 °C. The slides were then stained with 4',6-diamidino-2-phenylindole (DAPI) and mounted with Vecta fluorescent hard mounts (Vector Laboratories) for examination. Images were acquired using an Olympus FV10i confocal laser-scanning microscope (Olympus, Tokyo, Japan).

For immunohistochemistry, nonspecific antibody binding was blocked using 2% normal bovine serum for 40 minutes. Then, the sections were incubated with rabbit anti-S100 (dilution 1:500, Abcam, Cambridge, UK, ab34686) and rat anti-CD31 (dilution 1:50, Dianova, Cambridge, UK) overnight at 4 °C. The sections were then incubated with peroxidase-labeled anti-rabbit or anti-rat antibody (Histofine Simplestain Max PO (R); Nichirei, Tokyo, Japan) for 60 minutes at 37 °C. Immunoreactions were visualized using 3,3-diaminobenzidine tetrahydrochloride (Sigma), and the sections were counterstained with hematoxylin.

Immunohistochemistry and Quantification of Intra-epidermal Nerve Fibers

Frozen sections of mouse hind paws were subjected to immunohistochemistry for PGP9.5. Sections were blocked with 2% normal bovine serum. The sections were incubated with rabbit anti-PGP9.5 antibody (dilution 1:200, Abcam, ab108986) overnight at 4 °C, followed by incubation with peroxidase-labeled anti-rabbit antibody (Histofine Simplestain Max PO (R); Nichirei, Tokyo, Japan) for 60 minutes at 37 °C. The immunoreaction was visualized using 3,3′-diaminobenzidine tetrahydrochloride (Sigma). The sections were counterstained with hematoxylin. The intra-epidermal nerve fibers of each paw section were counted under 40× magnification in a blinded fashion, and the density of the fibers was calculated as fibers/mm.[22,23] The mean fiber density (n = 5 per group) was calculated from 5 mice.

Concentration Evaluation of Platinum

Tumor and dorsal root ganglion (DRG) issues for the assessment of platinum concentration were freshly dissected from mice (n = 4 each) and stored at –80 °C until analysis. The concentrations of total platinum, a surrogate marker for oxaliplatin levels, in dissected tumor tissues were homogenized and determined by ICP-MS (7,700x, Agilent Technology).

Scanning Electron Microscopy

Scanning electron microscopy was used to detect the three-dimensional microstructure of endothelial glycocalyx. Mice were anesthetized and perfused with lanthanum-containing alkaline solution according to previously described procedures.[16,24] Before perfusion, an incision was made in the right atrial appendage. A perfusion pump was used for injection at a steady rate of 1 mL/minute. The tissues were removed from the mice and fixed. Sample preparation for scanning electron microscopy was performed as described previously.[16,24]

Cell Culture and In Vitro Vascular Permeability Assay

Primary human dermal microvascular endothelial cells (adult) were purchased from Lonza (Catalog #: CC-2543). Cells were cultured in EBM-2 Basal Medium (CC-3156) supplemented with EGMTM-2MV Microvascular Endothelial Cell Growth Medium SingleQuots (CC-4147) (Lonza). All cells were maintained al 37 °C in a humidified 5% CO_2 atmosphere. The vascular permeability assay was performed according to the manufacturer's instructions (ECM644, Millipore). Briefly, primary human

dermal microvascular endothelial cells were seeded onto semi-permeable inserts pre-coated with collagen and cultured to confluency. The cells were treated either with vesicle, oxaliplatin and/or nafamostat for 24 hours. After 24 hours, the permeability treatment was removed and FITC-dextran was added to the semi-permeable insert coated with the human dermal microvascular endothelial cells for 60 minutes at room temperature. Subsequently, 100 μL of medium was collected from the receiver tray, transferred to 24-well plate, and read in the fluorescent plate reader at 485 nm and 535 nm for excitation and emission, respectively.

Statistical Analyses

The data presented represent the mean ± standard error of the mean of the repeat observation made before or after normalization to the baseline values. All experiments were performed in multiple replicates unless otherwise indicated and were repeated at least twice. Interaction between time (0, 2, 9, 16, 23, 30 days) and treatment groups was assessed using a two-way repeated measures analysis of variance (ANOVA). For pairwise comparisons between the control group and each treatment group, an unpaired two-sided Welch's t-test with the Bonferroni correction was applied. This correction multiplies the *P*-value by the number of treatment groups compared to the control. In all analysis, a two-sided *P*-value of $<.05$ was considered statistically significant. The data analyses were carried out using Graphpad Prism 10 and R software, version 4.4.2 (www.r-project.org).

Results

Blood-Nerve Barrier was Observed in the Subcutaneous Tissue of the Mouse Paw

Peripheral nerves are surrounded by 3 types of connective tissue, that is, the endoneurium, perineurium, and epineurium (Supplementary Fig 1A). In the peripheral nerve, individual nerve fascicles consisting of unmyelinated and myelinated axons, as well as small endoneurial blood vessels, were sheathed by the perineurium, forming the endoneurial microenvironment (Supplementary Fig 1A). These structures were observed in the peripheral tissues of mice and humans (Supplementary Fig 1B). The endothelial capillary vessels in the perineum were less than 10 μm in diameter. Blood was supplied by a network of capillary-like microvessels derived from microvascular arteries and veins, which are branches of large blood vessels in the extremities (Supplementary Fig 1C). The blood-nerve barrier is a physiological boundary separating the peripheral nerve axons from the bloodstream that prevents the transfer of substances from the plasma to the nerve fibers. Endothelial cells lining capillary microvessels are normally non-fenestrated with a layer of endothelial glycocalyx (Supplementary Fig 1C). Mononuclear cells and soluble factors, related to the loss of endothelial glycocalyx, crossing this microvascular barrier may trigger immune-mediated neuropathies.

Endothelial Glycocalyx was Disrupted in the Blood-Nerve Barrier in Oxaliplatin-Induced Neuropathy

It has been suggested that the breakdown of blood-nerve barrier drives the initial pathogenic events, leading to a multitude of inflammatory or immune-mediated neuropathies or neurodegenerative diseases.[25,26] Thus, it was hypothesized that direct exposure to oxaliplatin causes disruption of the endothelial glycocalyx, leading to breakdown of the blood-nerve barrier.

To investigate whether the breakdown of the blood-nerve barrier by oxaliplatin-induced neuropathy is associated with the disruption of endothelial glycocalyx, an oxaliplatin-induced neuropathology mouse model was established. After intraperitoneal administration of oxaliplatin (30 mg/kg/mouse) twice weekly for 5 weeks (Fig 1A), a significant interaction between time (0, 2, 9, 16, 23, 30 days) and treatment (control, oxaliplatin) in the paw withdraw threshold was revealed by two-way ANOVA ($P < .05$) (Fig 1B). Oxaliplatin-treated mice showed a significant hyperalgesic response, specifically mechanical allodynia, compared to untreated mice on days 2, 16, 23 and 30, as determined by the unpaired two-sided Welch's t-test ($P < .05$). Optical microscopic images showed that the subcutaneous nerves surrounding the perineurium in the paws of oxaliplatin-treated mice were slightly edematous compared to the untreated controls (Fig 1C), suggesting the onset of neuropathy. However, the nerves within the perineurium were extremely thin and the endoneurial capillary vessels were not well defined.

Thus, to clarify the microenvironment of the perineurium, including endothelial cells and endothelial glycocalyx, scanning electron microscopy with Lanthanum staining was used. The three-dimensional image showed peripheral nerves and capillaries adhering and running together in the paws of non-treated control mice. However, oxaliplatin-treated mice showed edema around the capillary vessels, and the peripheral nerves were frayed and disjointed (Fig 2A). In the endothelial glycocalyx in the lumen of the endoneurial capillary vessel, the untreated mice had more glycocalyx, while endothelial glycocalyx was almost lost in the mice treated with oxaliplatin (Fig 2A). These results indicate that the breakdown of endoneurial capillary vessels with the disruption of endothelial glycocalyx in the blood-nerve barrier may be the initial step in oxaliplatin-induced peripheral neuropathy (Fig 2B).

Nafamostat Mesilate Suppressed Mechanical and Cold Allodynia in Oxaliplatin-Induced Neuropathy

Nafamostat mesilate suppresses inflammation-induced degradation of endothelial glycocalyx and can have a beneficial effect on endothelial glycocalyx.[27]

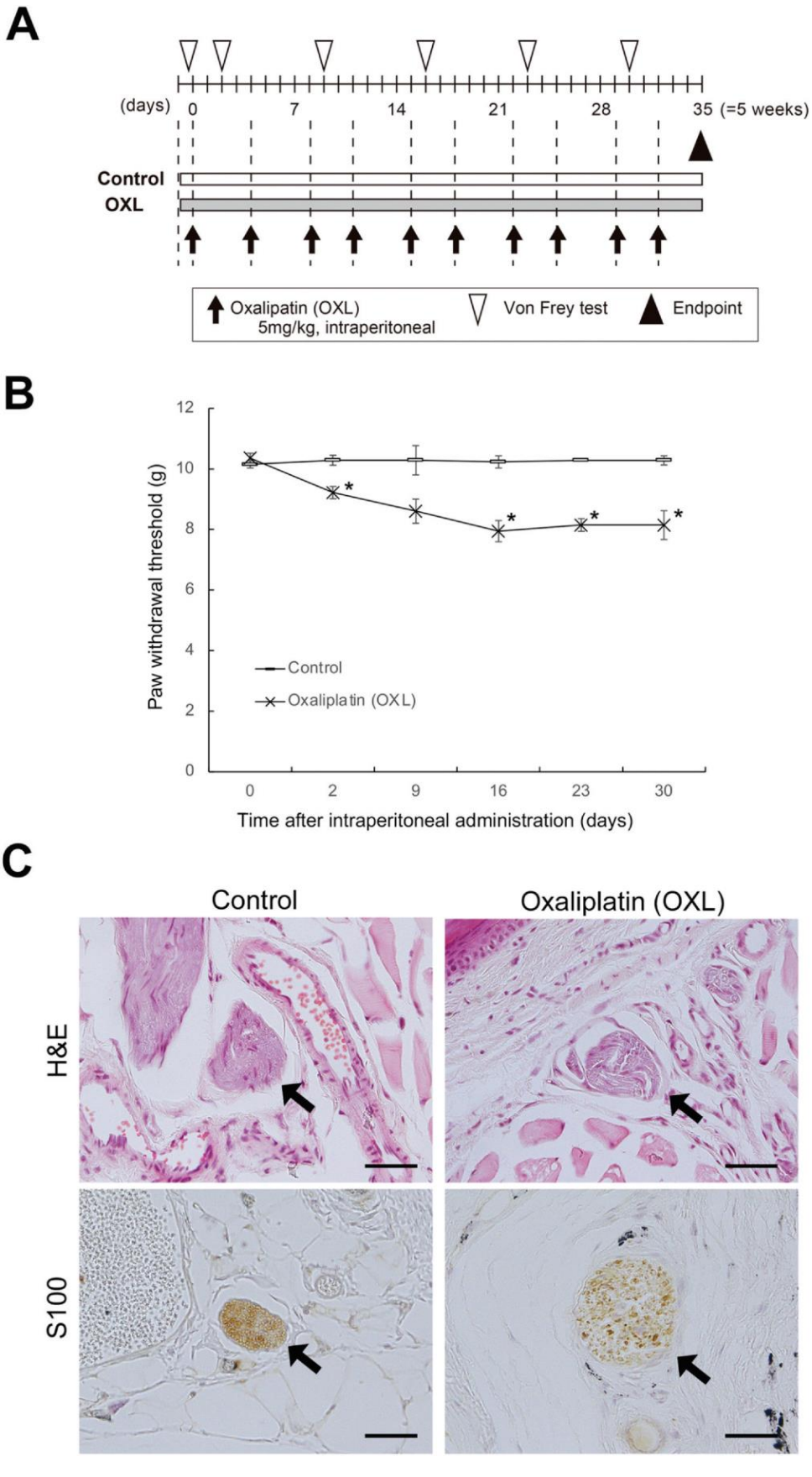

(caption on next page)

Figure 1. Endothelial glycocalyx injury in the blood-nerve barrier of the peripheral nerve in oxaliplatin-induced neuropathy (OIPN). **(A)** Experimental schedule of oxaliplatin (OXL) administration in mice. **(B)** The evaluation of paw withdrawal thresholds to mechanical stimulation (von Frey filament) between the no-treatment control and OXL-treated cohort (n = 5 each). Data are expressed as the means ± SEM. Interaction between time and treatment groups was assessed using a two-way repeated measures ANOVA. An unpaired two-sided Welch's t-test was applied for pairwise comparisons between the no-treatment control and OXL-treated cohort. *$P < .05$. **(C)** Hematoxylin and eosin staining and S100, a neuronal marker, images of the perineurium in the peripheral nerve. Arrows indicate the perineurium. Scale bars = 100 μm.

Therefore, nafamostat mesilate acts as a protective agent for endothelial glycocalyx.

To investigate the effects of different doses of nafamostat mesilate, mechanical allodynia was induced using the von Frey test as a preliminary short-term experiment. Different doses of nafamostat mesilate (0, 3, 10, and 30 mg/kg/day) were administered to the mice, together with a definite amount of oxaliplatin (Supplementary Fig 2). High doses of nafamostat mesilate (30 mg/kg) significantly inhibited the hyperalgesic response compared to the no-treatment group (0 mg) ($P < .05$) (Supplementary Fig 2). In this experiment, no mice with a nafamostat mesilate dose of 30 mg/kg showed no bleeding tendency or mortality. A nafamostat mesilate dose of 30 mg/kg was selected for subsequent experiments.

To determine whether drug treatments affected body weight, mice were weighed every 1 or every 2 weeks (Fig 3A). There was no significant interaction between time (0, 1, 3, 5, 7, 9 weeks) and treatment (control, oxaliplatin, nafamostat mesilate, oxaliplatin+nafamostat mesilate) in the body weight, as revealed by two-way ANOVA (Fig 3B). Only the oxaliplatin (G2) group had a lower final body weight than the initial body weight. The final body weights of mice in the control (G1), nafamostat mesilate (G3), and oxaliplatin+nafamostat mesylate (G4) treatment groups were higher than those of their initial body weights.

To investigate the effects of oxaliplatin and/or nafamostat mesilate on tumor progression, the tumor volume was measured at the indicated time points (Fig 3A). There was significant interaction between time (0, 1, 3, 5, 7, 9 weeks) and treatment (control, oxaliplatin, nafamostat mesilate, oxaliplatin+nafamostat mesilate) in tumor volume, as revealed by two-way ANOVA (Fig 3C). The colon tumors of control (G1) and the nafamostat mesilate (G3) treatment groups grew approximately 9 times larger than that at the beginning of treatment. Oxaliplatin (G2) and oxaliplatin +nafamostat mesilate (G4) treated groups had tumors that grew approximately 4 times larger compared to that at the start of treatment. Although the difference was not significant, tumor growth was lower at the endpoint in the oxaliplatin (G2) and oxaliplatin+nafamostat mesilate (G4) groups than in the control (G1) groups (Fig 3C).

To determine the effects of nafamostat mesilate on mechanical allodynia under tumor-bearing conditions in the right dorsal flank of the body, the variation of the paw withdrawal threshold was investigated using the von Frey test in all groups (Fig 3A). There was significant interaction between time (0, 1, 3, 5, 7, 9 weeks) and treatment (control, oxaliplatin, nafamostat mesilate, oxaliplatin+nafamostat mesilate) in paw withdraw threshold, as revealed by two-way ANOVA (Fig 3D). The oxaliplatin (G2) group showed a hyperalgesic response over time and, at the endpoint, was approximately 1.5 times higher compared to the beginning of oxaliplatin treatment (Fig 3D). At the endpoint, the oxaliplatin+ nafamostat mesilate (G4) group showed a level of hyperalgesic response similar to that in the control (G1) and nafamostat mesilate (G3) groups. The hyperalgesic response was significantly repressed in the oxaliplatin (G2) group compared to that in the control (G1) group on 1, 3, 5, 7 and 9 weeks, as revealed by the unpaired two-sided Welch's t-test ($P < .05$, Fig 3D). In contrast, there were no significant differences between the oxaliplatin+nafamostat mesilate (G4) group and the control (G1) group.

Next, to assess the effects of nafamostat mesilate on cold allodynia in OIPN, we conducted the acetone test. There was a tendency of interaction between time (0, 5, 11, 17, 23, 26 days) and treatment (control, oxaliplatin, oxaliplatin + nafamostat mesilate) in the paw withdraw threshold to oxaliplatin-induced cold hypersensitivity measured in the acetone test, as revealed by a two-way repeated measures ANOVA ($P = .090$) (Supplementary Fig 3). The cold hypersensitivity was significantly more pronounced in the oxaliplatin group than in the control group on days 17, 23, and 26, as determined by the unpaired two-sided Welch's t-test ($P < .05$). In contrast, no significant differences were observed between the oxaliplatin+nafamostat mesilate group and the control group (Supplementary Fig 3).

To determine the uptake of oxaliplatin in tumor tissues, the concentration of total platinum was measured as a surrogate marker for oxaliplatin levels in the control (G1), oxaliplatin (G2), and oxaliplatin+nafamostat mesilate (G4) groups. The concentration of oxaliplatin in tumor tissues was not inhibited in the oxaliplatin+nafamostat mesilate (G4) group compared to that in the oxaliplatin (G2) group (Fig 3E), suggesting that nafamostat mesilate does not suppress the drug delivery of oxaliplatin to tumor tissues. There was an increase in the concentration of oxaliplatin in the oxaliplatin+nafamostat mesilate (G4) treatment group compared to oxaliplatin (G2) group, albeit the difference between the groups was not significant.

Dorsal Root Ganglion is not Affected by Oxaliplatin and Nafamostat Treatment

The mechanism of OIPN involves both DRG and peripheral nerves. To determine whether oxaliplatin robustly accumulates in the DRGs, we measured the total platinum concentration in the DRGs of the control (G1), oxaliplatin (G2), and oxaliplatin+nafamostat mesilate (G4) groups. The concentration of oxaliplatin in the DRGs was not lower in the oxaliplatin+nafamostat mesilate (G4) group than that in the oxaliplatin (G2) group (Supplementary Fig 4), suggesting that nafamostat mesilate does not suppress the platinum accumulation, a surrogate marker of oxaliplatin, to DRGs in this model.

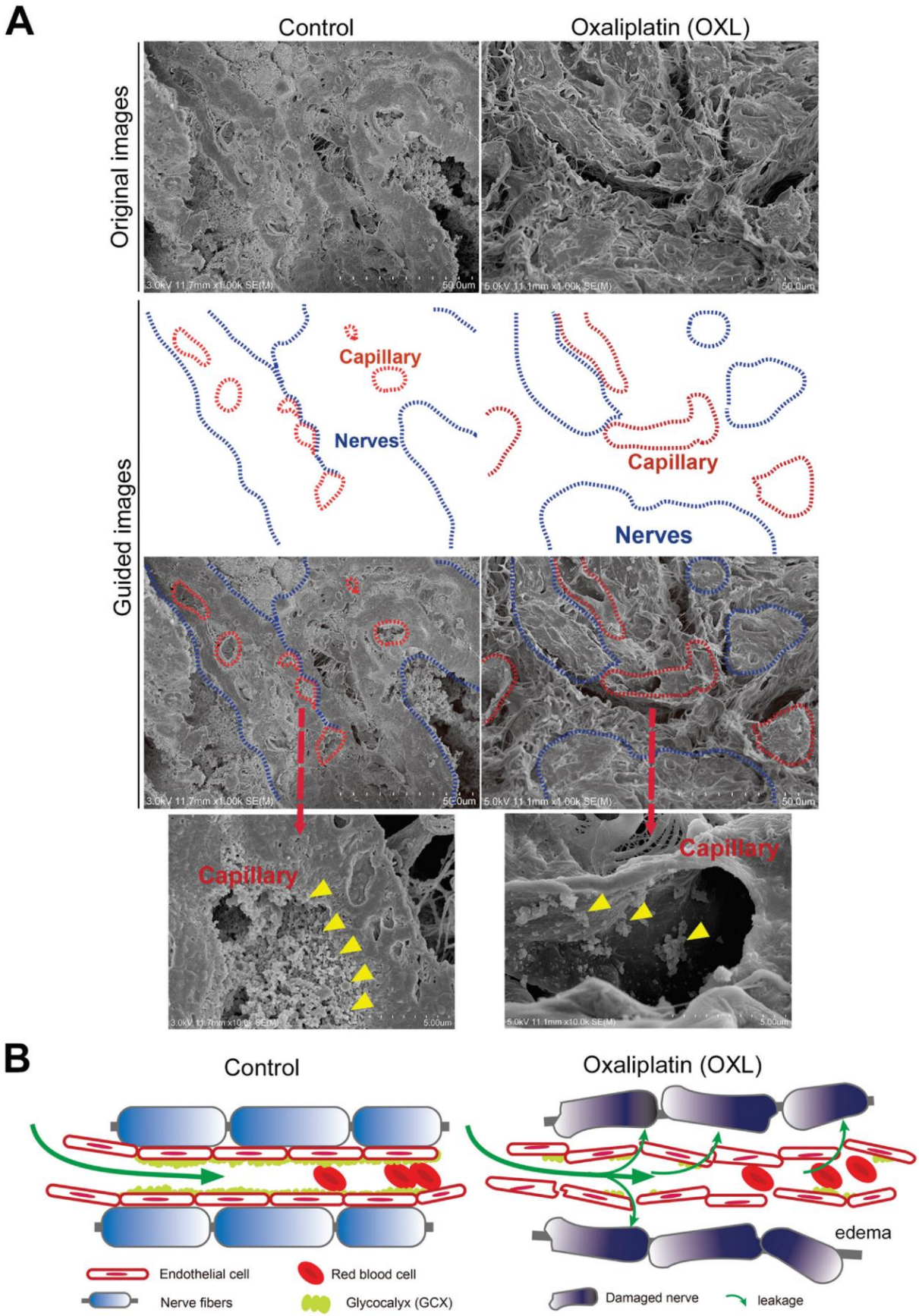

Figure 2. Three-dimensional images showing the disruption of the blood-nerve barrier in OIPN. **(A)** Representative scanning electron microscopy images of the blood-nerve barrier in subcutaneous nerves of the paw in no-treatment control (CON) and oxaliplatin (OXL)-treated mice. Lanthanum nitrate staining visualizes the endothelial glycocalyx. Blue and red dotted lines surround the nerves and capillary vessels, respectively. Green arrowheads indicate endothelial glycocalyx showing a moss-like shape. **(B)** Illustration of the endothelial glycocalyx in the blood-nerve barrier.

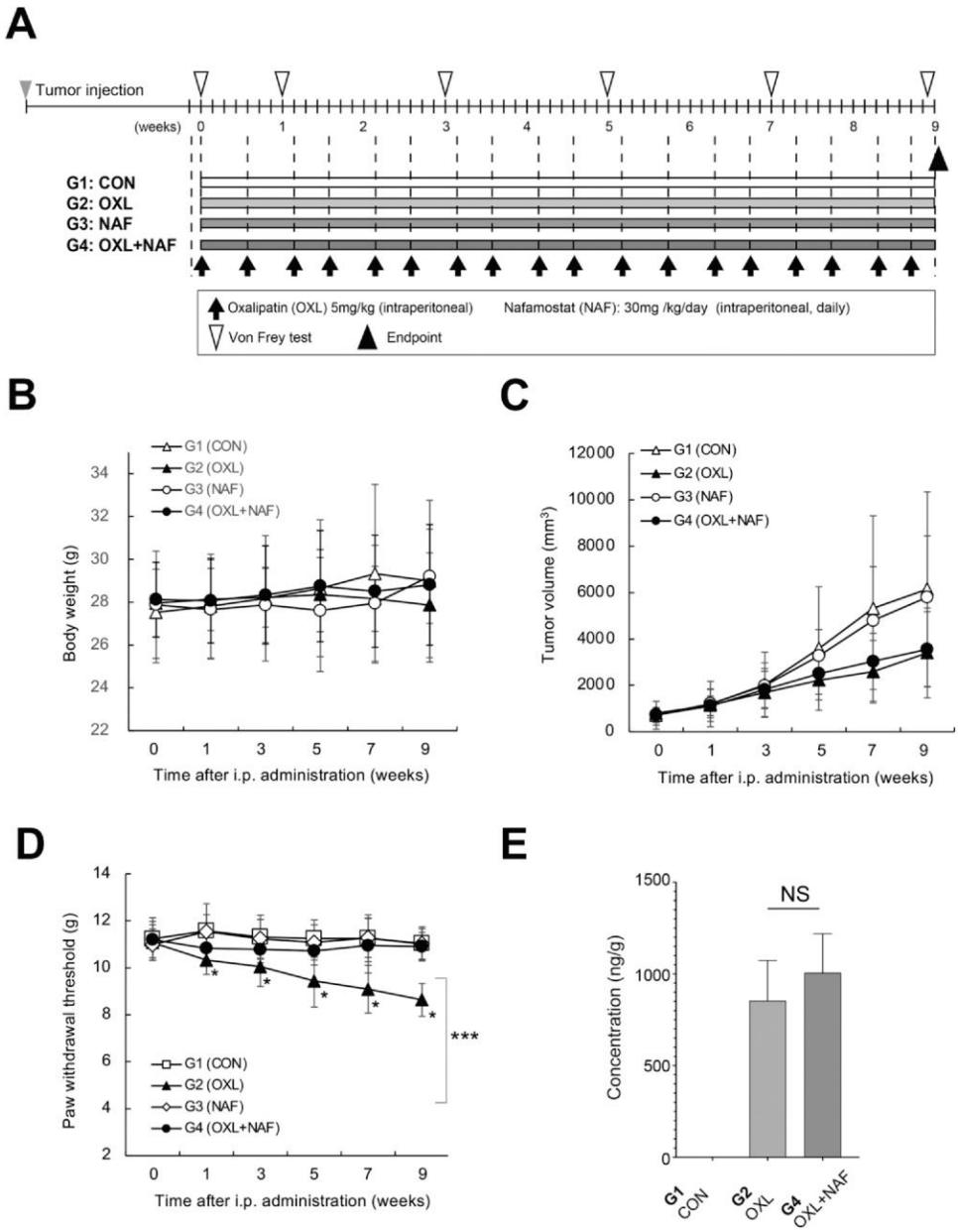

Figure 3. Nafamostat mesilate protection of OIPN without tumor progression. **(A)** Schematic diagram of the experimental protocol. CON, Control; OXL, oxaliplatin; NAF, Nafamostat. G1, Group 1; G2, Group 2; G3, Group 3; G4, Group 4. All the mice were euthanized at the study endpoint day. **(B)** Body weight (g), **(C)** tumor weight (g), and **(D)** paw withdrawal thresholds to mechanical stimulation (von Frey filament) were evaluated at the indicated time points. Data are expressed as the means ± SEM (Data of A–C in CON (G1) group, n = 10; OXL (G2) group, n = 10; NAF (G3) group, n = 10; OXL+NAF (G4) group, n = 10). Interaction between time and treatment groups was assessed using a two-way repeated measures ANOVA. An unpaired two-sided Welch's t-test with the Bonferroni correction was applied for pairwise comparisons between the control group and each treatment group. $*P < .05$, $***P < .0001$. **(E)** Quantification of platinum concentrations in tumor tissues in the CON (G1), OXL (G2), and OXL+NAF (G4) groups (n = 4 in each cohort). Data are expressed as means ± SEM. NS, not significant by Mann-Whitney U test.

Unexpectedly, there was an increase in the concentration of oxaliplatin in the oxaliplatin+nafamostat mesilate (G4) treatment group compared to oxaliplatin (G2) group, albeit the difference between the groups was not significant ($P = .057$ by Mann-Whitney U test).

Next, to assess the neuronal toxicity of oxaliplatin in the sensory neurons of the DRG tissues, we performed immunohistochemistry using the phosphorylated neurofilament heavy subunit (pNF-H) antibody. The loss of pNF-H immunoreactivity in DRG tissues corresponds to the relative neurotoxicity of oxaliplatin.[28] The results showed that the sensory neuron diameter and the loss of pNF-H immunoreactivity were not significantly different in the control (G1), oxaliplatin (G2), and oxaliplatin+nafamostat mesilate (G4) groups (Supplementary Fig 5).

Nafamostat Mesilate Prevented Intra-epidermal Nerve Fber Loss Related to Vascular Permeability

Mechanical allodynia induced by oxaliplatin is closely associated with loss of intra-epidermal nerve fiber (IENF)

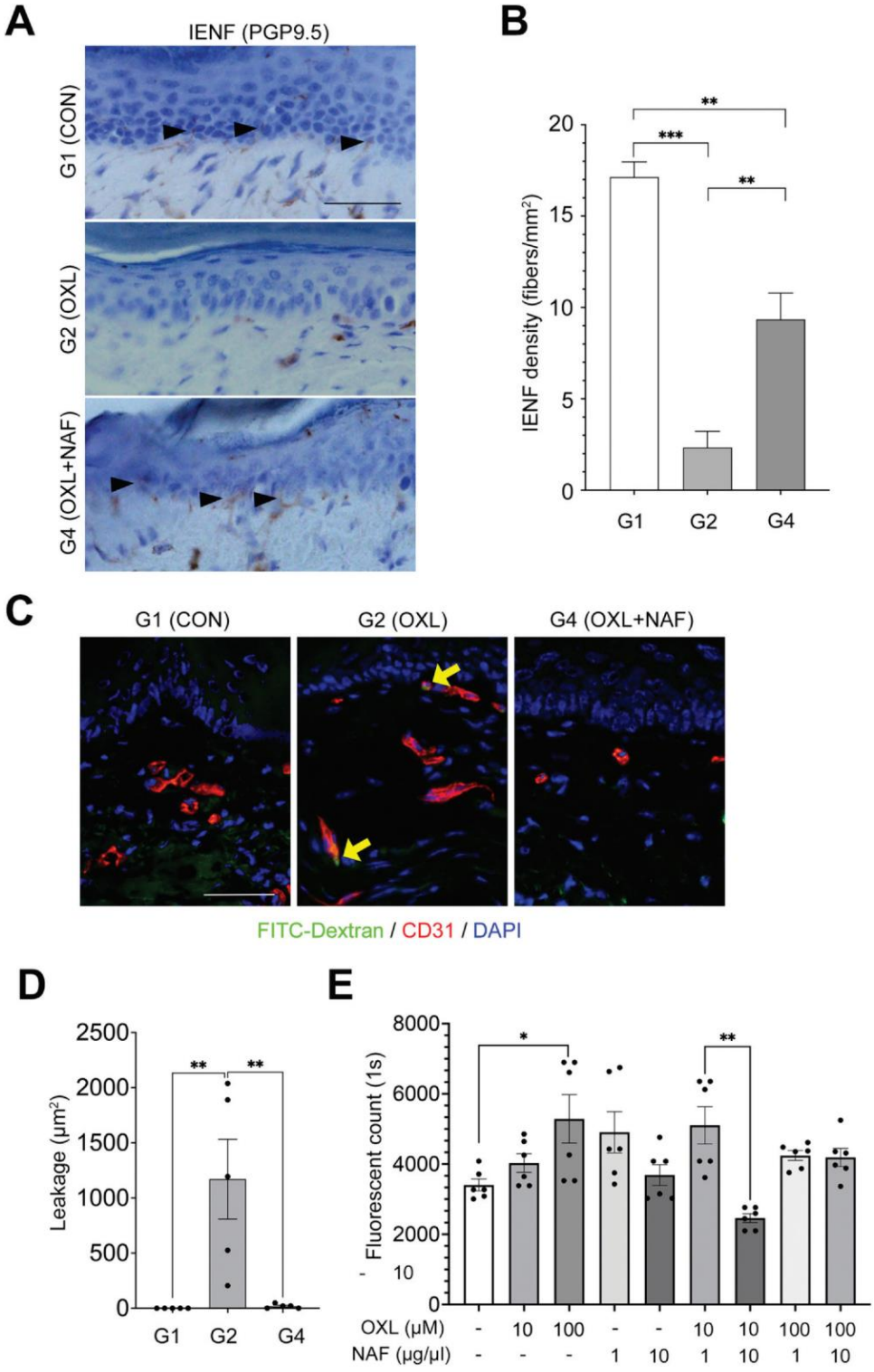

Figure 4. Nafamostat mesilate prevented dermal nerve fiber density and decreased vascular permeability in mice and human dermal endothelial cells. **(A)** Representative images of immunohistochemistry of PGP9.5 expression in subcutaneous tissue sections of paw specimens in control (CON) (G1), oxaliplatin (OXL) (G2), and OXL+nafamostat mesilate (NAF) (G4) groups. Arrowheads indicate nerve fibers entering into the epidermis. Scale bars = 50 μm. **(B)** Quantification of IENF density in each cohort (n = 4 each). Data are expressed as the means ± SEM. *$P < .05$; **$P < .01$; ***$P < .001$ by Mann-Whitney U test. **(C)** Subcutaneous tissue sections of the paw specimens in CON (G1), OXL (G2), and OXL + NAF (G4) groups. Sections in the mice with FITC-dextran (green) injected intravenously were stained for CD31 (red). Nuclei were stained with DAPI (blue). Arrows indicate the leakage of FITC-dextran from capillary vessel walls. Scale bars = 100 μm. **(D)** Leakage area (μm^2) of FITC-Dextran fluorescence in each cohort (on 2–3 images per mouse) was calculated using ImageJ software. Data represent values ± SEM. *$P < .05$; **$P < .01$ by Mann-Whitney U test. **(E)** Oxaliplatin induced-vascular hyperpermeability was inhibited by nafamostat in the human dermal microvascular endothelial-cell culture. The extravasation of FITC-Dextran in transwells with oxaliplatin and/or nafamostat-administrated monolayers of endothelial cells was measured at 24 hours and compared to those with monolayers of basal (unstimulated) endothelial cells. Data represent values ± SEM. *$P < .05$; **$P < .01$ by Mann-Whitney U test. 1 second.

loss.[22,23] To clarify the status of IENF in all groups, immunohistochemistry was performed to detect PGP9.5, a neural marker, and the IENF density was evaluated in hind paw samples dissected at the endpoint (35 days, Fig 3A). Conversely, the control (G1) group showed an even and abundant distribution of IENFs, which were almost absent in the oxaliplatin (G2) group (Fig 4A). The oxaliplatin (G2) group had significantly lower IENF density than the control (G1) and oxaliplatin+nafamostat mesilate (G4) groups (Fig 4B). Although there was a significant difference between the oxaliplatin (G2) and oxaliplatin+nafamostat mesilate (G4) groups, the latter group had a significantly higher IENF density than the oxaliplatin (G2) group (Fig 4B). These results indicate that nafamostat mesilate suppressed oxaliplatin-induced fiber loss in the skin.

Based on these results, it was hypothesized that nafamostat mesilate protects against and inhibits oxaliplatin-induced vascular injury in the peripheral paw based on the structure of the blood-nerve barrier, as shown in Supplementary Fig 1. To investigate the vascular permeability of the peripheral paws in the control (G1), oxaliplatin (G2), and oxaliplatin+nafamostat mesilate (G4) groups, FITC–dextran was injected intravenously and the capillary vessels were observed using immunofluorescent staining for CD31, an endothelial-cell marker. The permeability and leakage of FITC–dextran from the capillary vessels increased in the oxaliplatin (G2) group compared to those in the untreated control (G1) group (Fig 4C). Although the capillary vessels in the control (G1) group were characterized by well defined borders, the vessel borders in the oxaliplatin (G2) group were blurred and indistinct (Fig 4C), suggesting that oxaliplatin injured the capillary endothelial cells causing high permeability and extravascular leakage. Extravascular leakage of FITC–-dextran was significantly inhibited in the paws of mice in the oxaliplatin+nafamostat mesilate (G4) group compared with G1 and G2 groups ($P < .001$) (Fig 4D).

To evaluate the direct effects of nafamostat treatment against oxaliplatin-induced endothelial-cell disruption, we performed the vascular permeability assay in human dermal microvascular endothelial-cell culture. The results showed nafamostat suppressed the hyperpermeability induced by oxaliplatin in vitro (Fig 4E). Our data suggests that, at least, nafamostat directly suppress the oxaliplatin-induced vascular permeability in the human dermal endothelial-cell culture.

Nafamostat Mesilate Inhibited (Oxaliplatin)-Induced Endothelial Glycocalyx Disruption

To investigate the damage to endothelial glycocalyx, which is closely associated with vascular hyperpermeability, in the capillary vessels of the paws of the control (G1), oxaliplatin (G2), and oxaliplatin+nafamostat mesilate (G4) groups, DyLight 488-labeled Lycopersicon esculentum (Tomato) lectin was intravenously injected and the fluorescent intensity of the capillary vessels was evaluated by immunofluorescent staining of CD31 (Fig 5A). The expression of DyLight 488-labeled Tomato lectin on the surface of endothelial cells in the capillary vessels of the paws of the oxaliplatin (G2) group was lower than that in the control (G1) and oxaliplatin+nafamostat mesilate (G4) groups (Fig 5A). Furthermore, the quantitative analyses showed that the fluorescent intensity and thickness of the endothelial glycocalyx was significantly reduced in the oxaliplatin (G2) group compared with the control (G1) and oxaliplatin +nafamostat mesilate (G4) groups ($P < .05$) (Fig 5B).

To confirm the protective effects of nafamostat mesilate against endothelial glycocalyx in oxaliplatin-induced vascular injury, the three-dimensional scanning electron microscopy images of the capillary vessels of the control (G1), oxaliplatin (G2), and oxaliplatin+nafamostat mesilate (G4) paws were obtained. Peripheral nerves and capillaries showed adhering and merging in the control (G1) and oxaliplatin+nafamostat mesilate (G4) groups (Figure 6A). Conversely, the oxaliplatin (G2) group presented evidence of edema around the capillary vessels and the peripheral nerves were frayed and disjointed (Figure 6A). Endothelial glycocalyx was identified as neatly covering the entire surface of the capillary lumen in the control (G1) and oxaliplatin+nafamostat mesilate (G4) groups, but not in the oxaliplatin (G2) group. Furthermore, the shape of the endothelial glycocalyx in the oxaliplatin+nafamostat mesilate (G4) group was different from that in the control (G1) group (Figure 6A), which may indicate a difference between the original and repaired glycocalyx.

In addition, the quantitative analysis by using immunostaining for S100 antibody showed that the area of extravascular edema in control (G1) and oxaliplatin + nafamostat group (G4) significantly smaller than that in the oxaliplatin alone (G2) group ($P < .05$) (Fig 6B).

Discussion

The present study revealed that oxaliplatin induced endothelial glycocalyx injury in the hind paw and increased vascular permeability. In addition, protection of endothelial glycocalyx by nafamostat mesilate reduced symptoms of OIPN and was clearly visualized by three-dimensional scanning electron microscopy imaging. These findings suggest that oxaliplatin-induced endothelial glycocalyx injury may be involved in the progression of OIPN symptoms (Fig 7). This study introduces a novel strategy to prevent OIPN by protecting the endothelial glycocalyx and vascular endothelial cells, a concept not widely discussed in current literature.[29-31] It highlights the role of endothelial glycocalyx in maintaining capillary structure and function and its vulnerability to damage from oxaliplatin treatment.

The ultrastructure of the endothelial glycocalyx has been visualized in various normal organs[16,17] and diseases, including sepsis,[24,32] COVID-19,[33,34] cancer,[18] diabetes mellitus,[34] and other diseases[35,36] using three-dimensional images obtained using scanning electron microscopy with standing lanthanum. Under oxaliplatin injury, the ultrastructure of the endothelial glycocalyx were clearly visualized in this study.

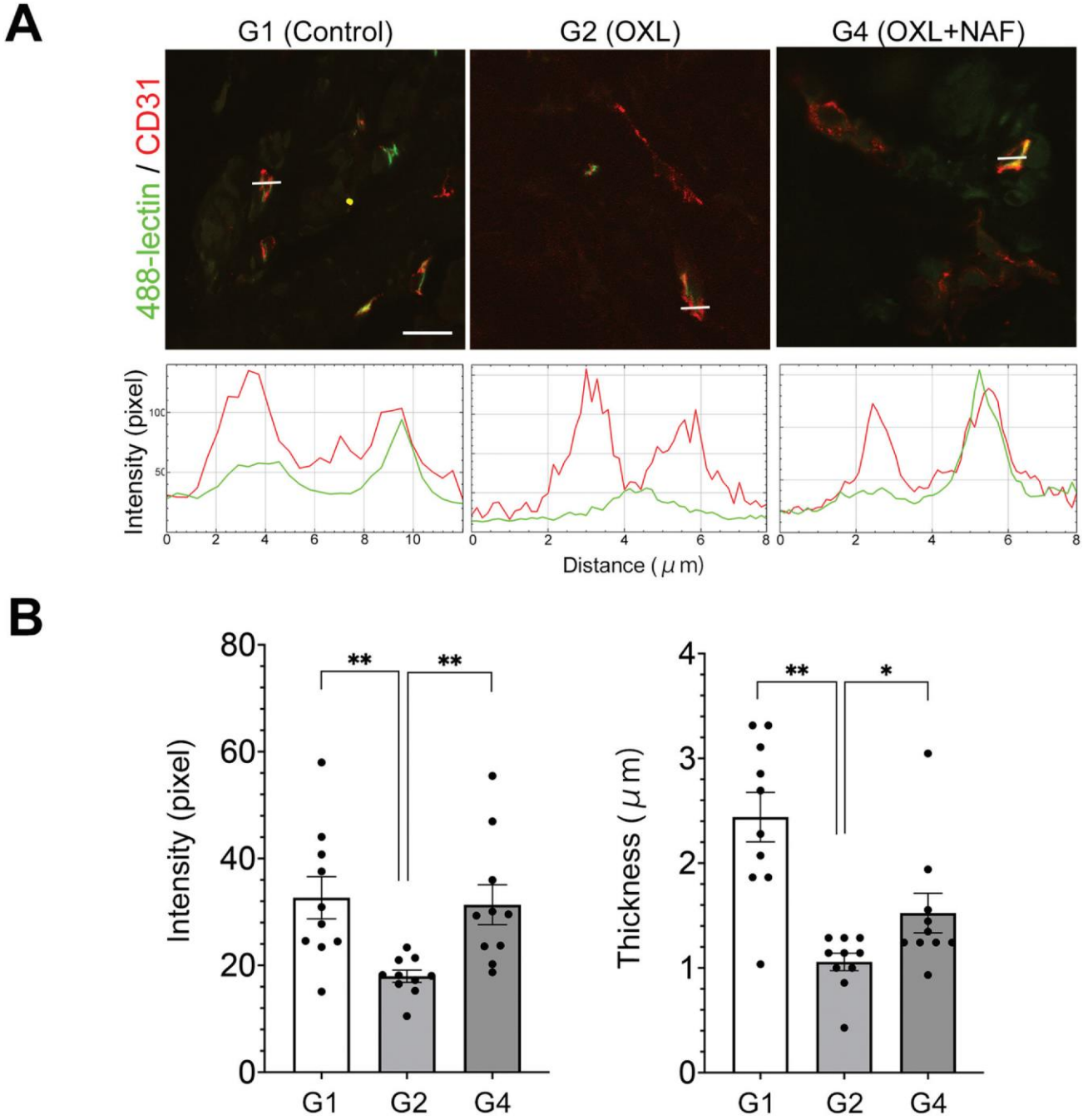

Figure 5. Nafamostat mesilate suppresses disruption of endothelial glycocalyx (glycocalyx) in the paw of oxaliplatin-treated mice. **(A)** Representative images illustrate the immunofluorescence staining findings of DyLight 488-Tomato lectin (green), which was injected intravenously, and CD31 (an endothelial-cell marker, antibody; red) in subcutaneous tissue sections of the paw in control (CON) (G1), oxaliplatin (OXL) (G2), and OXL+nafamostat mesylate (NAF) (G4) groups. The white line on the photo indicates where the intensity was measured. Scale bars = 50 μm. *(lower panels)* Shown is the distribution of the Dylight 488-Tomato lectin (green) in the vessel wall that is marked by CD31 (red). The intensity graphs of the capillary lumen and wall for each organ are also presented. Each graph indicates the intensity profile of the linear line in the corresponding image above it. **(B)** The intensity and thickness of the 488-lectin fluorescence in each cohort (on 2–3 images per mouse) was calculated using ImageJ software. Data represent values ± SEM. *$P < .05$; **$P < .01$ by Mann-Whitney U test.

Several studies using animal models have shown that endothelial injury occurs during the process of organ dysfunction, in which endothelial injury leads to microcirculatory dysfunction with subsequent organ ischemia and damage, including the brain, heart, lungs, liver, and kidneys; endothelial glycocalyx damage is thought to be the initial stage in endothelial injury.[16,32,24,37] This theory is also supported by several clinical studies.[38-41] In the relationship between sensory nerves and the endothelium, these closely interact starting from organogenesis and during development leading to the expression of their functions to maintain homeostasis. In addition, it is known that the endothelium and nerve networks anatomically present a branching pattern in which they are closely

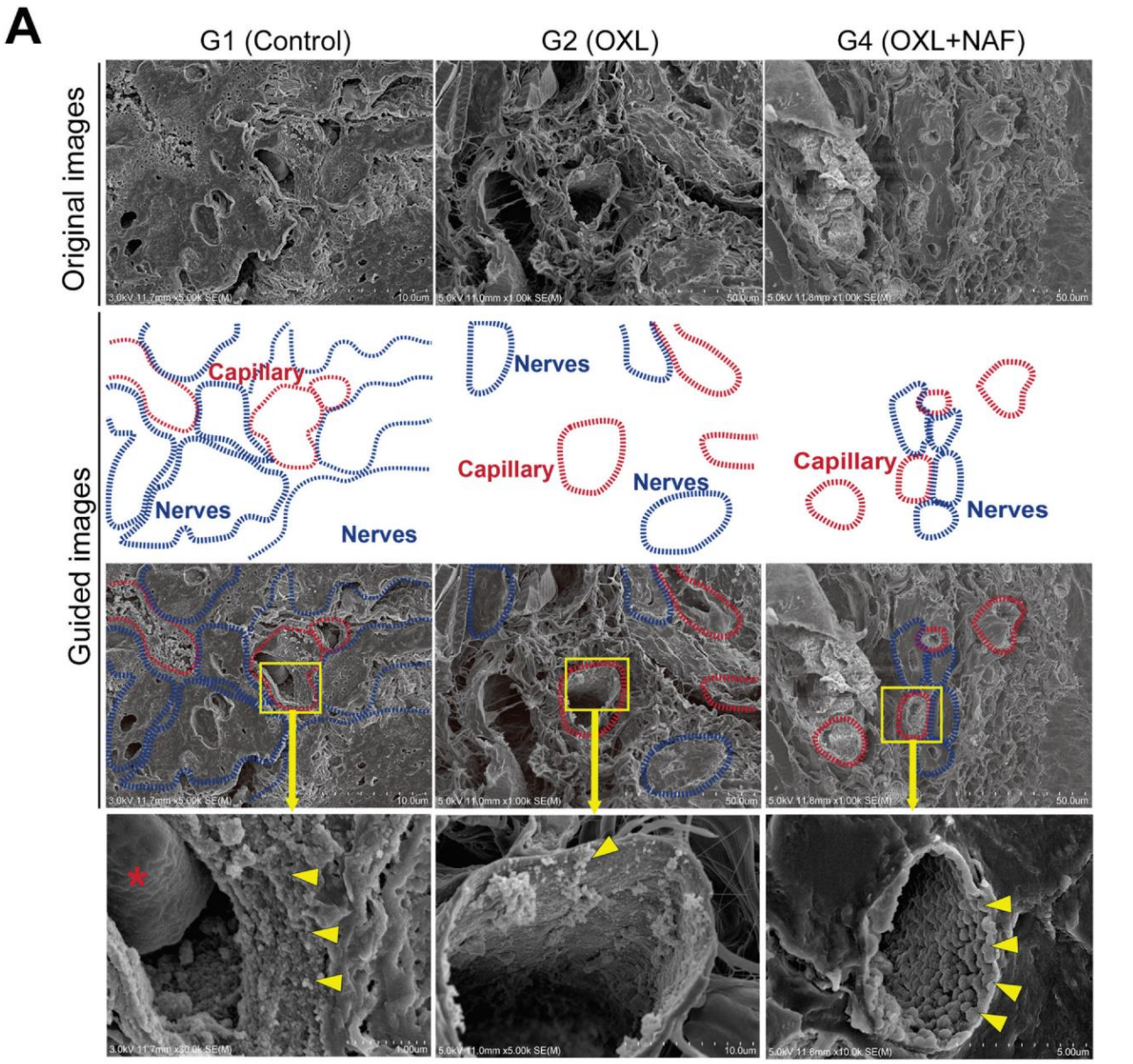

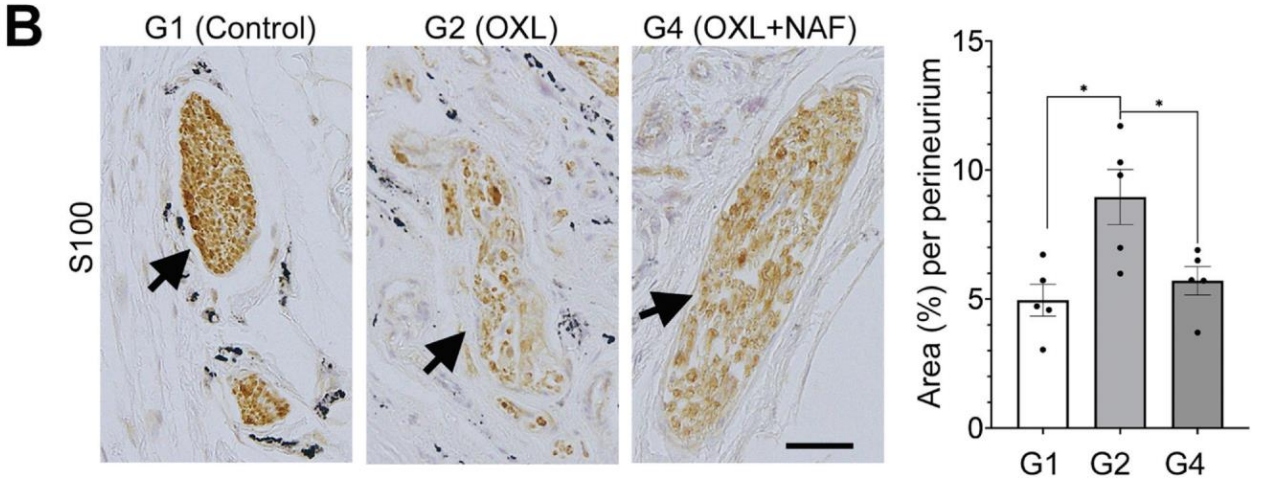

(caption on next page)

Figure 6. Nafamostat mesilate suppresses glycocalyx disruption and extravascular edema in the paw of oxaliplatin-treated mice. **(A)** Scanning electron microscopy images of the ultrastructure of the continuous capillaries in subcutaneous tissue sections of the paw in CON (G1), OXL (G2), and OXL+NAM (G4) groups. Lanthanum nitrate staining is used to visualize the endothelial glycocalyx. Blue and red dotted lines surrounding the nerves and capillary vessels, respectively. The rectangular area surrounded by yellow indicates the extent of the enlargement below. Yellow arrowheads indicate endothelial glycocalyx showing a moss-like shape. A red asterisk indicates a red blood cell in the endoneurial capillary. **(B)** Immunostaining for S100 antibody, a neuronal marker, images of the perineurium in the edema area of the perineurium in each cohort. The edema area (%) per a perineurium (on 2–3 images per mouse) was calculated using ImageJ software. Data represent values ± SEM. Data represent values ± SEM. *$P < .05$ by Mann-Whitney U test. Arrows indicate the perineurium.

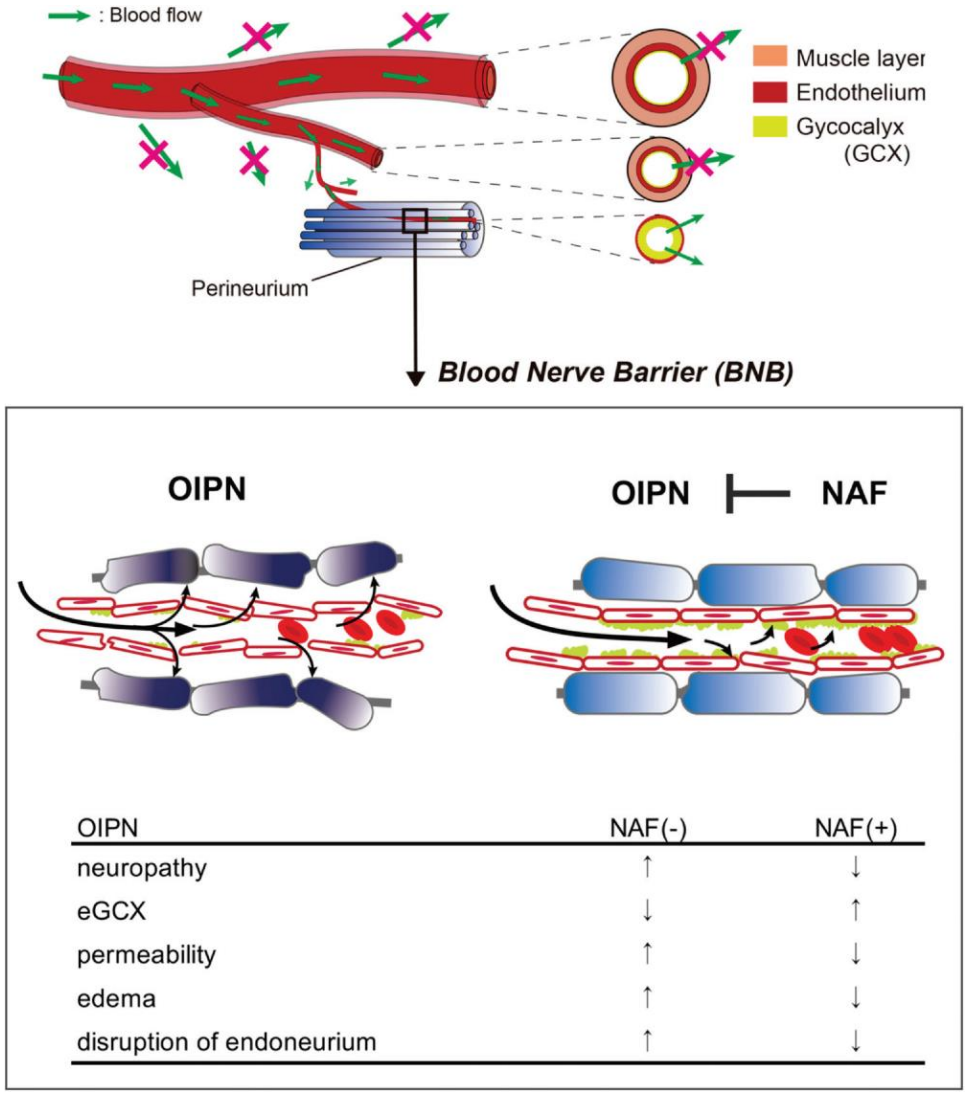

OIPN	NAF(-)	NAF(+)
neuropathy	↑	↓
eGCX	↓	↑
permeability	↑	↓
edema	↑	↓
disruption of endoneurium	↑	↓

Figure 7. Proposed new strategy for preventing OIPN and summary in this study.

aligned and run parallel.[42] In this study, using scanning electron microscopy imaging, the vascular endothelium and nerve fiber bundle in the hind paw of mice were shown to be anatomically in close proximity to each other, and based on the lectin staining findings, the endothelium with glycocalyx mediated the vascular permeability.

Mechanisms underlying OIPN have been extensively investigated in animal models but remain poorly understood. Acute-phase mechanisms involve alterations in neuronal voltage-gated Na^+,[43,44] K^+ (Kagiava et al, 2008), Ca^{2+}[45] channels, and transient receptor potential channels.[46] The chronic OIPN phase is attributed to DNA damage,[47] mitochondrial damage,[48,49] oxidative stress,[50,51] and platinum accumulation in neurons. Cellular uptake of platinum-based chemotherapeutics, including oxaliplatin, occurs via a facilitated transport mechanism.[52] Oxaliplatin effects are limited to organs capable of transporting it from the blood to cells.[53,54]

Similar to previous studies,[55-58] oxaliplatin administration in mice caused OIPN, as determined by the threshold of paw withdrawal following mechanical stimulation (von Frey filament) and nerve fiber damage in the hind paw, as evaluated by the IENFD assay. Furthermore, the present study clarified that endothelial glycocalyx in the hind paw was damaged by oxaliplatin administration, and the increased permeability of the

endothelium in the hind paw was evidenced by fluorescently labeled dextran. Edema was observed between the endothelium with injury to the glycocalyx and nerve fibers on scanning electron microscopy imaging.

There is now a general consensus that soluble small molecules such as chemotherapeutics move passively across the barrier via the paracellular route (Aird, 2007). Furthermore, in response to inflammation, postcapillary venules present increased permeability and inducible transfer of small molecules between endothelial cells (paracellular route) and endothelial cells (transcellular route).[59] Conversely, endothelial degradation of glycocalyx exposes underlying cell adhesion molecules, thus promoting adhesion of white blood cells, including leukocytes and platelet adhesion, and induces inflammatory responses.[60]

The effects of oxaliplatin-induced endothelial glycocalyx injury were also evaluated. The present study showed that nafamostat mesilate significantly reduced OIPN and evaluated paw withdrawal thresholds in response to mechanical stimulation (von Frey filament) without affecting antitumor effects. In particular, nafamostat mesilate suppressed glycocalyx injury and reduced nerve fiber damage and vascular permeability in the hind paw. Edema between the endothelium and injured glycocalyx and the nerve fibers were also suppressed. The protective effects of nafamostat mesilate were dose-dependent and were confirmed at concentrations greater than 5 mg/kg nafamostat mesilate.

Nafamostat mesilate, a synthetic serine protease inhibitor, is used for the treatment of disseminated intravascular coagulation, hemorrhagic lesions, acute pancreatitis, and the prevention of blood clot formation during extracorporeal circulation.[61-64] Nafamostat mesilate has been previously reported to inhibit the kallikrein-kinin system, which promotes vascular permeability through bradykinin.[65-67] Kusuzawa et al[27] described a retrospective observational study of 145 patients who underwent hemodialysis in which treatment with nafamostat mesilate inhibited the hemodialysis-induced increase in serum syndecan-1, which is a component of endothelial glycocalyx.

Therefore, these results may indicate that nafamostat mesilate suppressed endothelial glycocalyx injury by oxaliplatin in the hind paw, which led to reduced vascular permeability and subsequent reduction in oxaliplatin exposure to the nerve fibers. Reports focusing on microcirculatory disorders are limited. The present findings suggest a novel strategy targeting endothelial glycocalyx for the treatment or prevention of diseases and adverse events. Nafamostat mesilate, the glycocalyx protective agent used in this study, is currently in clinical use and its validity has been confirmed through drug repositioning; that is, its safety and pharmacokinetic profile in humans have already been confirmed. Many other candidate glycocalyx-protecting drugs, including anticoagulants, are currently used for the treatment of shock and severe inflammation. These drugs can be rapidly made available to humans via drug repositioning. Taken together, this study shows that nafamostat mesilate has extremely high potential as a safe and inexpensive glycocalyx-protective agent in some conditions.

The mechanism of OIPN involves both DRG and peripheral nerves. Historically, the predominant site of injury appeared to be the DRG, and a lot of experiments have been performed using DRG neurons in vitro. However, Martinez et al[68] recently reported no detectable DRG abnormalities after oxaliplatin treatment in a rat model, contrary to models of nerve injury. Immunohistochemistry analysis of sensory neuron damage in their study revealed that sensory neurons in the DRG are not affected by oxaliplatin treatment. Furthermore, Warncke et al[23] reported no significant differences in DRGs between oxaliplatin-treated C57BL6 mice and their naïve controls. These reports support our results that sensory neurons in the DRG are not affected by oxaliplatin treatment in our C57B6/J strain model. Together, the impairment of neurophysiological morphology and functions by oxaliplatin is distinctive among different strains of mice and careful consideration and selection of experimental models are necessary.

Regarding oxaliplatin effects, there is little sex difference in the tests used in this study on C57B6L/J mice.[23] This study was conducted solely in C57BL/J male mice to confirm the effects of nafamostat mesilate on the skin and other organs, excluding effects related to sex (given that female hormones are known to affect vascular endothelial glycocalyx). More detailed studies should be conducted in the future to demonstrate differences between the sexes.

Other limitation of the current study is that although changes in dextran leakage due to glycocalyx injury could be evaluated, the changes in oxaliplatin leakage could not be determined. In addition, the direct mechanisms underlying the oxaliplatin-induced glycocalyx injury or the preventive effect of nafamostat mesylate on the glycocalyx injury remain known. The mechanisms of oxalioplatin-induced injury and regeneration of endothelial glycocalyx require further study.

Conclusions

Oxaliplatin causes endothelial glycocalyx injury in the hind paw and increases vascular permeability, leading to the progression of OIPN symptoms. Additionally, nafamostat mesilate-induced endothelial glycocalyx protection inhibits the disruption of the microenvironment surrounding the blood-nerve barrier and reduces the symptoms of OIPN. These findings support a novel prophylactic strategy for OIPN treatment. Furthermore, these results demonstrate the effectiveness of drug repositioning as a promising treatment strategy that reduces the side effects of anticancer drugs. Cancer drug maximization therapy reduces side effects and allows the use of higher doses of anticancer drugs. This new perspective may change the approach to anticancer therapies and may help prevent the onset of side effects.

Conflicts of interest statement

The authors have no conflicts of interest.

Funding: This study was supported by JSPS KAKENHI JP20K0758723 (HT), JP23H03326 (HT), JP23K06276 (AS), and JST FOREST Program JPMJFR220W (H.T.).

Acknowledgments

We thank Chihiro Takada, Kyoko Takahashi, Ayako Suga, Reiko Kitazumia, and Izumi Toshima for their support. We would like to thank Editage (www.editage.com) for the English language editing.

Author Contributions

All authors contributed to this article as follows: conceptualization (T.K., A.S., H.O., H.T.); methodology (K.S., K.M., K.O., D. W.); formal analysis (M.S., A.N., Y.I., K.I., T.O., T.T., T.K., R.K., D.W.); investigation (K.S., K.M., K.O., A.N., Y.I., K.I., T.O., T.T., T.K., R.K.); technical assistance (M.S., T.O., T.T., T.K., R.K); visualization of data (K.O., K.M., H.O., H.T.); study supervision (S.S., A.H.); writing-original draft (T.K., A.S., H.O., H.T.); writing-review and editing (A.S., H.O., H.T.); critical review of the final manuscript (A.S., H.O., A.H., H.T.); obtaining resources (S.S.) and funding acquisition (H.T.). All authors have read and agreed to the order of appearance and published versions of the manuscript.

Appendix A. Supporting information

Supplementary data associated with this article can be found in the online version at doi:10.1016/j.jpain.2024.01.005.

References

1. De Falco V, Napolitano S, Rosello S, *et al.* How we treat metastatic colorectal cancer. ESMO Open 4:e000813, 2020.

2. Argyriou AA, Polychronopoulos P, Iconomou G, *et al.* Incidence and characteristics of peripheral neuropathy during oxaliplatin-based chemotherapy for metastatic colon cancer. Acta Oncol 46:1131-1137, 2007.

3. Hilkens PH, ven den Bent MJ: Chemotherapy-induced peripheral neuropathy. J Peripher Nerv Syst 2:350-361, 1997.

4. Park SB, Lin CS, Krishnan AV, *et al.* Dose effects of oxaliplatin on persistent and transient Na+ conductances and the development of neurotoxicity. PLoS One 6:e18469, 2011.

5. Yamazaki K, Nagase M, Tamagawa H, *et al.* Randomized phase III study of bevacizumab plus FOLFIRI and bevacizumab plus mFOLFOX6 as first-line treatment for patients with metastatic colorectal cancer (WJOG4407G). Ann Oncol 27:1539-1546, 2016.

6. Peng S, Ying AF, Chan NJH, *et al.* Prevention of oxaliplatin-induced peripheral neuropathy: a systematic review and meta-analysis. Front Oncol 12:731223, 2022.

7. Malong L, Napoli I, Casal G, *et al.* Characterization of the structure and control of the blood-nerve barrier identifies avenues for therapeutic delivery. Dev Cell 58:174-191 e178, 2023.

8. Richner M, Ferreira N, Dudele A, *et al.* Functional and structural changes of the blood-nerve-barrier in diabetic neuropathy. Front Neurosci 12:1038, 2018.

9. James JM, Mukouyama YS: Neuronal action on the developing blood vessel pattern. Semin Cell Dev Biol 22:1019-1027, 2011.

10. Saffari TM, Mathot F, Bishop AT, Shin AY: New methods for objective angiogenesis evaluation of rat nerves using microcomputed tomography scanning and conventional photography. Microsurgery 40:370-376, 2020.

11. Weinbaum S, Tarbell JM, Damiano ER: The structure and function of the endothelial glycocalyx layer. Annu Rev Biomed Eng 9:121-167, 2007.

12. Komarova Y, Malik AB: Regulation of endothelial permeability via paracellular and transcellular transport pathways. Annu Rev Physiol 72:463-493, 2010.

13. Jin J, Fang F, Gao W, *et al.* The structure and function of the glycocalyx and its connection with blood-brain barrier. Front Cell Neurosci 15:739699, 2021.

14. Yang R, Chen M, Zheng J, Li X, Zhang X: The role of heparin and glycocalyx in blood-brain barrier dysfunction. Front Immunol 12:754141, 2021.

15. Zhu J, Li Z, Ji Z, *et al.* Glycocalyx is critical for blood-brain barrier integrity by suppressing caveolin1-dependent endothelial transcytosis following ischemic stroke. Brain Pathol 32:e13006, 2022.

16. Ando Y, Okada H, Takemura G, *et al.* Brain-specific ultrastructure of capillary endothelial glycocalyx and its possible contribution for blood brain barrier. Sci Rep 8:17523, 2018.

17. Suzuki A, Tomita H, Okada H: Form follows function: the endothelial glycocalyx. Transl Res 247:158-167, 2022.

18. Tachi M, Okada H, Matsuhashi N, *et al.* Human colorectal cancer infrastructure constructed by the glycocalyx. J Clin Med 8:1270, 2019.

19. Pozzi E, Fumagalli G, Chiorazzi A, *et al.* The relevance of multimodal assessment in experimental oxaliplatin-induced peripheral neurotoxicity. Exp Neurol 334:113458, 2020.

20. Brenner DS, Golden JP, Gereau RWt: A novel behavioral assay for measuring cold sensation in mice. PLoS One 7:e39765, 2012.

21. Decosterd I, Woolf CJ: Spared nerve injury: an animal model of persistent peripheral neuropathic pain. Pain 87:149-158, 2000.

22. Boyette-Davis J, Dougherty PM: Protection against oxaliplatin-induced mechanical hyperalgesia and intraepidermal nerve fiber loss by minocycline. Exp Neurol 229:353-357, 2011.

23. Warncke UO, Toma W, Meade JA, *et al.* Impact of dose, sex, and strain on oxaliplatin-induced peripheral neuropathy in mice. Front Pain Res ((Lausanne)) 2:683168, 2021.

24. Okada H, Takemura G, Suzuki K, *et al.* Three-dimensional ultrastructure of capillary endothelial glycocalyx under normal and experimental endotoxemic conditions. Crit Care 21:261, 2017.

25. Nelson AR, Sweeney MD, Sagare AP, Zlokovic BV: Neurovascular dysfunction and neurodegeneration in dementia and Alzheimer's disease. Biochim Biophys Acta 1862:887-900, 2016.

26. Sweeney MD, Sagare AP, Zlokovic BV: Blood-brain barrier breakdown in Alzheimer disease and other neurodegenerative disorders. Nat Rev Neurol 14:133-150, 2018.

27. Kusuzawa K, Suzuki K, Okada H, *et al.* Measuring the concentration of serum syndecan-1 to assess vascular endothelial glycocalyx injury during hemodialysis. Front Med 8:791309, 2021.

28. Jamieson SM, Subramaniam J, Liu JJ, *et al.* Oxaliplatin-induced loss of phosphorylated heavy neurofilament subunit neuronal immunoreactivity in rat DRG tissue. Mol Pain 5:66, 2009.

29. Cheng F, Zhang R, Sun C, *et al.* Oxaliplatin-induced peripheral neurotoxicity in colorectal cancer patients: mechanisms, pharmacokinetics and strategies. Front Pharmacol 14:1231401, 2023.

30. Egashira N: Pathological mechanisms and preventive strategies of oxaliplatin-induced peripheral neuropathy. Front Pain Res 2:804260, 2021.

31. Yang Y, Zhao B, Gao X, *et al.* Targeting strategies for oxaliplatin-induced peripheral neuropathy: clinical syndrome, molecular basis, and drug development. J Exp Clin Cancer Res 40:331, 2021.

32. Inagawa R, Okada H, Takemura G, *et al.* Ultrastructural alteration of pulmonary capillary endothelial glycocalyx during endotoxemia. Chest 154:317-325, 2018.

33. Okada H, Yoshida S, Hara A, Ogura S, Tomita H: Vascular endothelial injury exacerbates coronavirus disease 2019: the role of endothelial glycocalyx protection. Microcirculation 28:e12654, 2021.

34. Sampei S, Okada H, Tomita H, *et al.* Endothelial glycocalyx disorders may be associated with extended inflammation during endotoxemia in a diabetic mouse model. Front Cell Dev Biol 9:623582, 2021.

35. Okamoto H, Muraki I, Okada H, *et al.* Recombinant antithrombin attenuates acute respiratory distress syndrome in experimental endotoxemia. Am J Pathol 191:1526-1536, 2021.

36. Suzuki K, Okada H, Takemura G, *et al.* Recombinant thrombomodulin protects against LPS-induced acute respiratory distress syndrome via preservation of pulmonary endothelial glycocalyx. Br J Pharmacol 177:4021-4033, 2020.

37. Schmidt EP, Yang Y, Janssen WJ, *et al.* The pulmonary endothelial glycocalyx regulates neutrophil adhesion and lung injury during experimental sepsis. Nat Med 18:1217-1223, 2012.

38. Kitagawa Y, Kawamura I, Suzuki K, *et al.* Serum syndecan-1 concentration in hospitalized patients with heart failure may predict readmission-free survival. PLoS One 16:e0260350, 2021.

39. Liborio AB, Braz MB, Seguro AC, *et al.* Endothelial glycocalyx damage is associated with leptospirosis acute kidney injury. Am J Trop Med Hyg 92:611-616, 2015.

40. Schmidt EP, Li G, Li L, *et al.* The circulating glycosaminoglycan signature of respiratory failure in critically ill adults. J Biol Chem 289:8194-8202, 2014.

41. Suzuki K, Okada H, Sumi K, *et al.* Serum syndecan-1 reflects organ dysfunction in critically ill patients. Sci Rep 11:8864, 2021.

42. Takara K, Hayashi-Okada Y, Kidoya H: Neurovascular interactions in the development of the vasculature. Life 13:42, 2022.

43. Paques EP, Romisch J: Comparative study on the in vitro effectiveness of antithrombotic agents. Thromb Res 64:11-21, 1991.

44. Sittl R, Lampert A, Huth T, *et al.* Anticancer drug oxaliplatin induces acute cooling-aggravated neuropathy via sodium channel subtype Na(V)1.6-resurgent and persistent current. Proc Natl Acad Sci USA 109:6704-6709, 2012.

45. Grolleau F, Gamelin L, Boisdron-Celle M, *et al.* A possible explanation for a neurotoxic effect of the anticancer agent oxaliplatin on neuronal voltage-gated sodium channels. J Neurophysiol 85:2293-2297, 2001.

46. Nassini R, Gees M, Harrison S, *et al.* Oxaliplatin elicits mechanical and cold allodynia in rodents via TRPA1 receptor stimulation. Pain 152:1621-1631, 2011.

47. Ta LE, Espeset L, Podratz J, Windebank AJ: Neurotoxicity of oxaliplatin and cisplatin for dorsal root ganglion neurons correlates with platinum-DNA binding. Neurotoxicology 27:992-1002, 2006.

48. Xiao WH, Zheng H, Bennett GJ: Characterization of oxaliplatin-induced chronic painful peripheral neuropathy in the rat and comparison with the neuropathy induced by paclitaxel. Neuroscience 203:194-206, 2012.

49. Zheng H, Xiao WH, Bennett GJ: Functional deficits in peripheral nerve mitochondria in rats with paclitaxel- and oxaliplatin-evoked painful peripheral neuropathy. Exp Neurol 232:154-161, 2011.

50. Ito N, Sakai A, Miyake N, *et al.* miR-15b mediates oxaliplatin-induced chronic neuropathic pain through BACE1 down-regulation. Br J Pharmacol 174:386-395, 2017.

51. Tsutsumi K, Yamashita Y, Ushio S, *et al.* Oxaliplatin induces hypomyelination and reduced neuregulin 1 expression in the rat sciatic nerve. Neurosci Res 80:86-90, 2014.

52. Sprowl JA, Ness RA, Sparreboom A: Polymorphic transporters and platinum pharmacodynamics. Drug Metab Pharmacokinet 28:19-27, 2013.

53. Jong NN, Nakanishi T, Liu JJ, Tamai I, McKeage MJ: Oxaliplatin transport mediated by organic cation/carnitine transporters OCTN1 and OCTN2 in overexpressing human embryonic kidney 293 cells and rat dorsal root ganglion neurons. J Pharmacol Exp Ther 338:537-547, 2011.

54. Zhang S, Lovejoy KS, Shima JE, *et al.* Organic cation transporters are determinants of oxaliplatin cytotoxicity. Cancer Res 66:8847-8857, 2006.

55. Cerles O, Benoit E, Chereau C, *et al.* Niclosamide inhibits oxaliplatin neurotoxicity while improving colorectal cancer therapeutic response. Mol Cancer Ther 16:300-311, 2017.

56. Chiorazzi A, Wozniak KM, Rais R, *et al.* Ghrelin agonist HM01 attenuates chemotherapy-induced neurotoxicity in rodent models. Eur J Pharmacol 840:89-103, 2018.

57. Kim S, Gang J, Lee JH, *et al.* [6]-Shogaol attenuates oxaliplatin-induced allodynia through serotonergic receptors and GABA in the spinal cord in mice. Pharmaceuticals 15:726, 2022.

58. Zhang P, Lu Y, Yang C, *et al.* Based on systematic pharmacology: molecular mechanism of siwei jianbu decoction in preventing oxaliplatin-induced peripheral neuropathy. Neural Plast 2020:8880543, 2020.

59. Aird WC: Phenotypic heterogeneity of the endothelium: I. Structure, function, and mechanisms. Circ Res 100:158-173, 2007.

60. Patterson EK, Cepinskas G, Fraser DD: Endothelial glycocalyx degradation in critical illness and injury. Front Med 9:898592, 2022.

61. Akizawa T, Koshikawa S, Ota K, *et al.* Nafamostat mesilate: a regional anticoagulant for hemodialysis in patients at high risk for bleeding. Nephron 64:376-381, 1993.

62. Makino S, Egi M, Kita H, *et al.* Comparison of nafamostat mesilate and unfractionated heparin as anticoagulants during continuous renal replacement therapy. Int J Artif Organs 39:16-21, 2016.

63. Minakata D, Fujiwara SI, Ikeda T, *et al.* Comparison of gabexate mesilate and nafamostat mesilate for disseminated intravascular coagulation associated with hematological malignancies. Int J Hematol 109:141-146, 2019.

64. Piascik M, Rydzewska G, Milewski J, *et al.* The results of severe acute pancreatitis treatment with continuous regional arterial infusion of protease inhibitor and antibiotic: a randomized controlled study. Pancreas 39:863-867, 2010.

65. Fujii S, Hitomi Y: New synthetic inhibitors of C1r, C1 esterase, thrombin, plasmin, kallikrein and trypsin. Biochim Biophys Acta 661:342-345, 1981.

66. Hitomi Y, Ikari N, Fujii S: Inhibitory effect of a new synthetic protease inhibitor (FUT-175) on the coagulation system. Haemostasis 15:164-168, 1985.

67. Park SR, Kim MJ, Nam BH, *et al.* A randomised phase II study of continuous versus stop-and-go S-1 plus oxaliplatin following disease stabilisation in first-line chemotherapy in patients with metastatic gastric cancer. Eur J Cancer 83:32-42, 2017.

68. Martinez NW, Sanchez A, Diaz P, *et al.* Metformin protects from oxaliplatin induced peripheral neuropathy in rats. Neurobiol Pain 8:100048, 2020.